

The Star Formation and AGN luminosity relation: Predictions from a semi-analytical model

Thales A. Gutcke^{1*}, Nikos Fanidakis¹, Andrea V. Macciò¹, & Cedric Lacey²

¹ *Max-Planck-Institut für Astronomie, Königstuhl 17, 69117 Heidelberg, Germany*

² *Institute for Computational Cosmology, Department of Physics, University of Durham, South Road, Durham, DH1 3LE, UK*

9 November 2021

ABSTRACT

In a universe where AGN feedback regulates star formation in massive galaxies, a strong correlation between these two quantities is expected. If the gas causing star formation is also responsible for feeding the central black hole, then a positive correlation is expected. If powerful AGNs are responsible for the star formation quenching, then a negative correlation is expected. Observations so far have mainly found a mild correlation or no correlation at all (i.e. a flat relation between star formation rate (SFR) and AGN luminosity), raising questions about the whole paradigm of “AGN feedback”. In this paper, we report the predictions of the **GALFORM** semi-analytical model, which has a very strong coupling between AGN activity and quenching of star formation. The predicted SFR-AGN luminosity correlation appears negative in the low AGN luminosity regime, where AGN feedback acts, but becomes strongly positive in the regime of the brightest AGN. Our predictions reproduce reasonably well recent observations by Rosario et al., yet there is some discrepancy in the normalisation of the correlation at low luminosities and high redshifts. Though this regime could be strongly influenced by observational biases, we argue that the disagreement could be ascribed to the fact that **GALFORM** neglects AGN variability effects. Interestingly, the galaxies that dominate the regime where the observations imply a weak correlation are massive early-type galaxies that are subject to AGN feedback. Nevertheless, these galaxies retain high enough molecular hydrogen contents to maintain relatively high star formation rates and strong infrared emission.

Key words:

1 INTRODUCTION

A clear understanding of how galaxies transition from star-forming disks to passive spheroidals is one of the open problems in the current paradigm of galaxy formation. One of the most widely accepted theories requires a large energy injection into the cores of massive galaxies; such energy will then heat up the cold gas in the center and prevent the accretion of new gas onto the galaxy. The most likely source for such energy are active galactic nuclei (AGN), powered by matter accretion onto super massive black holes (SMBHs) at the centers of galaxies (Silk & Rees 1998).

In the last decade both semi-analytical models and numerical simulations have tried to incorporate such an effect into the modelling of galaxy formation. Semi-analytical models have showed that if the energy from AGN is coupled

to the hot and cold gas, it is indeed possible to halt star formation and create passive galaxies (Kauffmann & Haehnelt 2000; Cattaneo 2001; Granato et al. 2004; Bower et al. 2006; Croton et al. 2006; Somerville et al. 2008; Fanidakis et al. 2011; Guo et al. 2011). Numerical simulations have also helped to shed light onto the interplay between a galaxy and its SMBH (e.g. Springel et al. 2005a; Di Matteo et al. 2005; Robertson et al. 2006; Sijacki et al. 2007; Hopkins et al. 2007; Di Matteo et al. 2008; Okamoto et al. 2008; Booth & Schaye 2009). More recently, large fully cosmological simulations including the effect of AGN feedback have been quite successful in reproducing properties of observed galaxies, including the luminosity function and star formation rate (Vogelsberger et al. 2014 and Schaye et al. 2015). There is general agreement that AGN feedback is a needed ingredient in galaxy formation and evolution.

These studies imply a strong correlation between the evolution of a galaxy and its central black hole. A hint to

* thales@mpia.de

such a correlation might reside in the so called M-sigma relation, namely the observed correlation between the velocity dispersion of the bulge of the galaxy and the mass of the supermassive black hole hosted by it (Ferrarese & Merritt 2000; Gebhardt et al. 2000, but see Jahnke & Macciò 2011 for a different explanation).

Another possible piece of evidence of a causal link between the rising of AGN activity and the quenching of a galaxy can be obtained by studying the observed correlation between star formation rate (SFR) and AGN luminosity (Shao et al. 2010, Lutz et al. 2010 and Harrison et al. 2012).

Recently, Rosario et al. 2012 used deep infrared and X-ray observations in the COSMOS, GOODS-NORTH and GOODS-SOUTH fields to estimate the SFR and AGN luminosity, respectively. They found a weak correlation between SFR and AGN activity at all redshifts, suggesting little connection between SF and BH growth in these systems, especially at high redshift and low luminosity. Mullaney et al. 2012b and Stanley et al. 2015 find a similar absence of correlation (but see Mullaney et al. 2012a and Rodighiero et al. 2015 for a possible correlation of SMBH growth rate and SFR).

This quite unexpected lack of correlation between SFR and AGN luminosity has been used to put constraints on the triggering of AGN activity and black hole growth (Neistein & Netzer 2014), possibly suggesting strong variability in AGN activity on time scales shorter than those typical of star formation, which are of the order 100 Myrs (Hickox et al. 2014).

In this paper, we take a deeper look into the expected correlation between SFR and AGN activity. We present predictions from the **GALFORM** semi-analytical model of galaxy formation (Cole et al. 2000) in which AGN feedback is the key ingredient to explain the fading of star formation in massive galaxies. **GALFORM** has been successful in reproducing a number of fundamental relations of galaxy evolution and structure: the luminosity and stellar mass functions of galaxies, the AGN diversity and evolution, the evolution of Lyman- α emitters (LAEs) and Lyman-break galaxies (LBGs), the number counts of sub-millimeter galaxies (SMGs), as well as the HI and HII mass functions (Baugh et al. 2005, Bower et al. 2006, Fanidakis et al. 2011, Lacey et al. 2011 and Lagos et al. 2012).

Using the version of **GALFORM** presented in Fanidakis et al. 2012 and assuming full co-evolution between the galaxy and its central BH, we study the predicted correlation between SF and AGN luminosity and compare it to observations and previous models of this relation. We stress that this correlation is not used as a constraint on the model, but presents a pure prediction of a model constrained by other observations.

The paper is organised as follows. In Section 1, we introduce the **GALFORM** semi-analytical model and describe the most important model ingredients that are relevant for this study. In Section 2, we present the predictions of the model for the FIR luminosity as a function of AGN activity and compare to the observations. In Section 3 we look at the molecular gas content of our galaxies to understand the material that is causing star formation. Finally, in Section 4, we discuss our findings and present our conclusions.

2 THE MODEL

Semi-analytic modelling in galaxy formation is used to simulate large numbers of galaxies in a computationally efficient manner, thus enabling statistical insight into the predictions of different galaxy formation models. It uses our understanding of cosmological structure formation in N-body simulations and adds a set of coupled differential equations to describe the physical processes of galaxy formation and evolution, making possible the analysis of a wide variety of galaxy and BH properties. **GALFORM**, one of the most extensively applied semi-analytical models, has been improved upon over time (Cole et al. 2000; Baugh et al. 2005; Bower et al. 2006; Fanidakis et al. 2011; Lagos et al. 2011) to include processes and adjustments that describe more accurately the formation and evolution of galaxies. Among the most important physical processes that are modelled in **GALFORM** are: i) the formation and evolution of DM haloes in the Λ CDM cosmology, ii) gas cooling and disk formation in DM haloes, iii) star formation, supernovae feedback and chemical enrichment, iv) BH growth and AGN feedback, v) and the formation of bulges through galactic disk instabilities and galaxy mergers.

The model is successful in reproducing many observations, including the luminosity and stellar mass functions of galaxies, the number counts of submillimeter galaxies, the evolution of Ly α and Ly-break galaxies, H and H₂ mass functions and the AGN diversity and evolution (Baugh et al. 2005; Bower et al. 2006; Orsi et al. 2008; Kim et al. 2011; Lacey et al. 2011; Lagos et al. 2011; Lagos et al. 2012; Lagos et al. 2014a; Lagos et al. 2014b; Fanidakis et al. 2011; Fanidakis et al. 2012; Fanidakis et al. 2013a; Fanidakis et al. 2013b; Gonzalez-Perez et al. 2013; Gonzalez-Perez et al. 2014). The model provides a very good fit to the HERSCHEL far-IR galaxy luminosity functions (LFs) and number counts (Lacey et al. in prep.; see also Lacey et al. 2010) and X-ray LFs of AGN in the $z = 0 - 3$ universe (Fanidakis et al. 2012; Fanidakis et al. in prep.) and therefore it is an ideal tool for studying the correlation between SFR and AGN activity.

For the purposes of this analysis, we use a version of the Fanidakis et al. (2012) model, updated to the cosmological parameters estimated by the 7-year data release of WMAP (Komatsu et al. 2011 and the Lacey et al. in prep. **GALFORM** model). The fundamental predictions of the model for the AGN properties are described in Fanidakis et al. (2013a,b, see also Fanidakis et al. in prep.). The predictions presented in this analysis are calculated using merger trees extracted from the DM only N-body simulation Millennium WMAP-7 (Lacey et al. in prep.). The Millennium WMAP-7 simulation has almost the same mass resolution ($8.61 \times 10^8 M_{\odot}$), particle number (10^7) and box size ($500 h^{-1}$ Mpc) as the Millennium simulation (Springel et al. 2005b) and differs only in the background cosmology (which is in agreement with WMAP7 results). We now describe in the rest of this section the main model processes and ingredients that are essential for understanding the **GALFORM** predictions for the SFR and AGN activity.

2.1 The two regimes of black holes growth

GALFORM assumes two regimes of black hole (BH) growth in galaxies. The first one is the “starburst” regime, where a galaxy experiences a starburst and AGN activity with high star formation and BH accretion rates. The high efficiency both in SF and BH growth of this regime is due to efficient gas cooling in DM haloes with masses lower than $5 \times 10^{12} M_{\odot}$. The onset of the starburst mode is triggered by either a merger or by a disk instability. In this regime, a fraction of the cold gas that turns into stars is accreted directly onto the BH. When only this regime is active, we expect a positive correlation between star formation rate (SFR) and active galactic nucleus (AGN) luminosity.

In the “hot-halo” regime, the growth of BHs is tightly linked to the AGN feedback mechanism and the suppression of gas cooling in haloes typically more massive than $5 \times 10^{12} M_{\odot}$. The gas feeding the BH during this mode is assumed to originate directly from the hot halo around the galaxy. The resulting accretion power is then coupled via a jet to the thermodynamical properties of the gas in the host halo and suppresses cooling, if the available heating power exerts the cooling luminosity of the gas, L_{cool} . Galaxies that are subject to AGN feedback still exhibit some SF, due to remaining cold gas and new gas brought in by mergers, but it is expected to be lower than in actively SF galaxies. In this regime, we expect a negative correlation between SFR and (AGN) luminosity.

In addition to the starburst and hot-halo modes of BH growth, BH-BH mergers during galaxy encounters also contribute to the growth of BHs. However, this growth mode only redistributes the BH mass and does not add new baryons to the BHs.

2.2 Bolometric accretion luminosity

The gas accreted during the starburst mode is converted into an accretion rate, \dot{M} , by assuming that the accretion duration is proportional to the dynamical timescale of the host spheroid,

$$\dot{M} = \frac{M_{\text{acc}}}{f_{\text{q}} t_{\text{bulge}}}. \quad (1)$$

Here M_{acc} is fixed for every galaxy to 0.5 percent of the mass that turns into stars during a starburst, t_{dyn} is the dynamical timescale of the host spheroid and f_{q} is a proportionality factor set to 10 in Fanidakis et al. (2012). In contrast, in the hot-halo mode, the accretion rate onto the BH is calculated directly from the cooling properties of the host DM halo, i.e.

$$\dot{M} = \frac{L_{\text{cool}}}{\epsilon_{\text{kin}} c^2}, \quad (2)$$

where ϵ_{kin} is the average kinetic efficiency of the jet during the AGN feedback. L_{cool} is the quasi-hydrostatic cooling luminosity of the halo. This is chosen assuming that the flow will balance heating and cooling in the hot halo mode (i.e. if the Eddington ratio is sufficiently large.) This accretion mode is associated with early type galaxies in massive haloes, with relatively low SFRs. Since the accretion process is responsible for shutting down SF in the host galaxy, a negative correlation between AGN luminosity and SFR is expected in this mode.

The bolometric luminosity of the accretion flow, L_{bol} , is calculated by assuming the Shakura-Sunyaev thin disk model (Shakura & Sunyaev 1973):

$$L_{\text{bol,TD}} = \epsilon \dot{M} c^2. \quad (3)$$

We assume that this solution is valid for accretion rates higher than 1 percent of the Eddington accretion rate, i.e. $\dot{m} = \dot{M}/\dot{M}_{\text{Edd}} \geq 0.01$, where \dot{M}_{Edd} is defined as $L_{\text{Edd}}/\epsilon c^2$. For lower accretion rates, the advection-dominated accretion flow (ADAF) thick-disk solution is used (Narayan & Yi 1994; Mahadevan 1997),

$$L_{\text{bol,ADAF}} = 0.44 \left(\frac{\dot{m}}{0.01} \right) \epsilon \dot{M} c^2. \quad (4)$$

When the accretion becomes substantially super-Eddington ($L_{\text{bol}} \geq \eta L_{\text{Edd}}$), the bolometric luminosity is limited to (Shakura & Sunyaev 1973):

$$L_{\text{bol}}(\geq \eta L_{\text{Edd}}) = \eta [1 + \ln(\dot{m}/\eta)] L_{\text{Edd}}, \quad (5)$$

where η is an ad hoc parameter, which we choose equal to 4, to allow a better modelling of the bright end of the AGN luminosity function (see Fanidakis et al. 2012). However, the accretion rate, \dot{m} , is not restricted if the flow becomes super-Eddington.

2.3 Star formation rate

Lagos et al. (2011) recently revised the original formulation of the SF law in GALFORM (Cole et al. 2000), in favour of the observationally motivated (and constrained) Blitz & Rosolowsky (Blitz & Rosolowsky 2006) empirical law. The Blitz & Rosolowsky law is motivated by UV, FIR and millimetre observations of SF and molecular gas in spiral galaxies and assumes that the surface density of star formation rate (SFR) is proportional to the surface density of molecular hydrogen in the disk.

$$\Sigma_{\text{SFR}} = \nu_{\text{SF}} \Sigma_{\text{mol}}. \quad (6)$$

The proportionality factor, ν_{SF} , is given as an inverse time scale and its value is closely constrained by observations. At every timestep, GALFORM calculates the molecular-to-atomic hydrogen ratio in the disk, R_{mol} , which is expressed as a power law of the internal hydrostatic pressure of the disk (Elmegreen 1993):

$$R_{\text{mol}} = \frac{\Sigma(\text{H}_2)}{\Sigma(\text{H})} = \left(\frac{P_{\text{ext}}}{P_0} \right)^{\alpha}. \quad (7)$$

Eq. 6 is then re-written in terms of the cold gas surface density, Σ_{gas} , as:

$$\Sigma_{\text{SFR}} = \nu_{\text{SF}} f_{\text{mol}} \Sigma_{\text{gas}}, \quad (8)$$

where $f_{\text{mol}} = R_{\text{mol}}/(1 + R_{\text{mol}})$. Integration of Eqn. 8 over the assumed exponential surface density profile of the gas gives the SFR of the galaxy.

When the galaxy experiences a burst of SF, triggered either by a galaxy-galaxy merger or a disk instability, the model assumes that the entire cold gas reservoir of the galaxy (atomic and molecular) is converted into stars. The SF timescale in starbursts is finite and proportional to the dynamical timescale of the host bulge. At a given time, we estimate the total SFR in the galaxy as the sum of the quiescent SFR and burst SFR.

2.4 Stellar and dust emission

GALFORM includes a self-consistent model for calculating the stellar emission in every galaxy and its absorption and re-emission in the mid and far-IR (8 – 1000 μm) and sub-mm wavelengths by dust. The model is similar in outline to the spectro-photometric model **GRASIL** (Silva et al. 1998), with some simplifications that speed-up significantly the calculation. The stellar emission in the model is calculated based on the stellar population synthesis model of Bressan et al. (1998) and assuming that the stars have an axisymmetric distribution in the disk and bulge. Dust in the galaxies is assumed to be a two-phase medium, i.e. diffuse low-density dust in the ISM and dense dust clouds enshrouding star forming regions. The amount of dust in each galaxy is determined by the total mass and metallicity of cold gas. The attenuation of stellar light by the dust is computed by interpolating the tabulated radiative transfer models of Ferrara et al. 1999. The FIR emission from the dust is calculated assuming that the cloud and diffuse dust components re-emit the absorbed starlight (i.e. the difference between the stellar and dust attenuated SED, integrated over wavelength) as a modified blackbody. This constrains the dust temperature (constant within a galaxy and different for each component), which is then used to calculate the SED of each dust component. The total dust SED is then found by summing over the SEDs of the two components. This technique works well for wavelengths greater than $\sim 60\mu\text{m}$.

The composite SED of stellar and dust emission of galaxies in **GALFORM** provides a very good fit to galaxy number counts and luminosity function in the FIR (see Lacey et al. in prep.). Here we are interested in comparing the predictions of the model directly to far-IR observations of AGN with the Herschel/PACS instrument, at a mean rest-frame wavelength of $60\mu\text{m}$. For model galaxies predicted by **GALFORM**, the monochromatic luminosity $\nu L_{60\mu\text{m}} = \nu L_{\nu}(60\mu\text{m})$ is typically $\sim 0.65L_{\text{IR}}$, where L_{IR} is the total FIR luminosity, defined as the integrated luminosity between 8 and 1000 μm . This wavelength range includes the entire emission from dust, while excluding the intrinsic stellar emission. In the rest of the analysis, the **GALFORM** predictions will be presented at $60\mu\text{m}$, unless the comparison with observational data requires a different band or the total dust emission. We note that the galaxy SED predicted by **GALFORM** does not include any AGN emission. Therefore, the dust emission predicted by the model is purely reprocessed stellar emission.

Finally, we note that the SFR is usually traced by emission in the FIR as the SFR is not a direct observable. As a first test, we check how good of a proxy this emission is for the actual SFR in our model. Fig. 1 shows the median IR luminosity at $60\mu\text{m}$ (blue line) and its 10th and 90th percentile (green shaded areas) as a function of SFR at $z = 0$ and $z = 2.1$. For high redshifts, the correlation is tighter, but even at $z = 0$ it is still present over several orders of magnitude. The positive dependence of L_{IR} on SFR is a consequence of the higher UV luminosity caused by the young stars. This in turn increases the dust heating and IR emission. At high SFRs, the $60\mu\text{m}$ emission seems to be directly proportional to the SFR. At intermediate and low SFRs (SFR $\lesssim 10^1 - 10^2 M_{\odot}\text{yr}^{-1}$) the correlation deviates mildly from a slope of unity mainly due to a somewhat lower

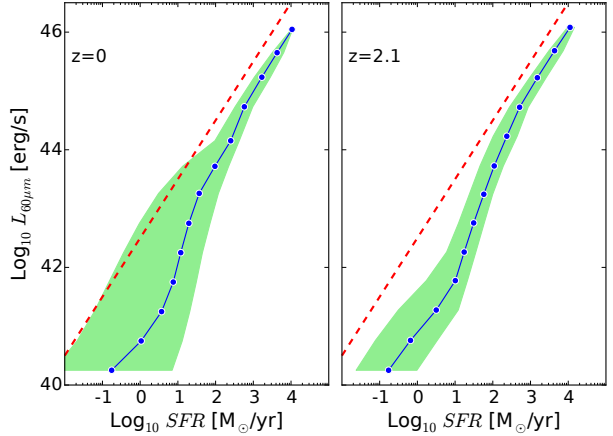


Figure 1. Predicted FIR emission at $60\mu\text{m}$ as a function of star formation rate (SFR) at $z = 0$ and $z = 2.1$. The solid lines show median values, and the shaded areas the 10th and 90th percentiles. The red dashed line shows a line with a slope of unity and an arbitrary normalization.

dust extinction or lower dust temperature. Overall, we can conclude that the FIR emission strongly couples to the SFR, thus, IR luminosity can be used as a proxy for SFR. We will henceforth use the FIR emission at $\nu L_{60\mu\text{m}}$ as a proxy of star formation (SF).

3 THE FIR–AGN LUMINOSITY CORRELATION

In this study we are interested in comparing the predicted and observed FIR–AGN luminosity correlations. Our final aim is to check what correlation of observable quantities is predicted by a model where AGN feedback is the driving mechanism for quenching star formation in high mass galaxies.

3.1 Model Predictions

We show our first predictions for the FIR–AGN luminosity correlation in Fig. 2, where we plot the distribution of galaxies on the $L_{\text{bol}} - \nu L_{60\mu\text{m}}$ plane. These galaxies represent a small subset (4,000) of the total sample (usually of the order of 10^6 galaxies) and are randomly selected from the model output at $z = 2.1$. We split our sample into galaxies undergoing active starburst AGN activity (cold-gas accretion, blue points) and galaxies whose BHs are in the hot halo mode (hot-gas accretion, red points). We also divide the sample by stellar mass, with galaxies of $M_{\star} > 10^{10} M_{\odot}$ marked by a larger symbol, to aid the reader in finding the trends in galaxies that are more likely to be observed. Interestingly, low luminosity objects accreting in the hot-halo mode show a negative trend of $\nu L_{60\mu\text{m}}$ with AGN luminosity. In contrast, high luminosity AGN, powered through the starburst mode, show a clear positive trend. The two different trends are a manifestation of the fact that each of the two accretion modes is linked to a different regime of SF efficiency.

The different trends are due to the two different modes in which a BH accretes gas. Large AGN luminosities are

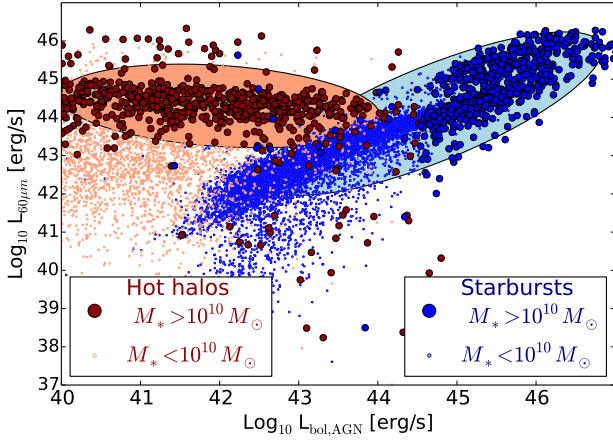


Figure 2. Predicted FIR emission at 60 μm , $\nu L_{60\mu\text{m}}$, as a function of bolometric AGN luminosity, L_{bol} , for 4,000 randomly selected galaxies at $z = 2.1$ (both centrals and satellites). Galaxies in which the central BH experiences starburst-mode activity are shown with blue, while those with BHs growing during the hot-halo mode with red. The point size indicates stellar masses below (small) and above (big) $10^{10} M_{\odot}$.

due to accretion of cold gas and mostly happen in haloes with masses below $\sim 5 \times 10^{12} M_{\odot}$, as shown in Fanidakis et al. (2013b). In this case, the triggering mechanism (galaxy mergers or disk instabilities) of cold-gas flows that feed the central BH is also responsible for a burst of SF in the host galaxy, hence the positive correlation. Low luminosity AGN mainly live in high mass haloes ($\gtrsim 10^{13} M_{\odot}$), where the gas fuelling the BH is accreted directly from the hot halo around the host galaxy (see Section 2). Accretion activity in this mode is tightly linked to the AGN feedback mechanism and, thus, is responsible for the suppression of gas cooling and SF. The quenching nature of this mode gives rise to a negative correlation. In summary, the intrinsic $\nu L_{60\mu\text{m}}$ vs L_{AGN} correlation predicted by GALFORM is entirely shaped by the physics of each of the accretion modes that are responsible for growing the central BH.

3.2 Comparison with Data

To compare our predictions with observational data, we show in Fig. 3 the average $\nu L_{60\mu\text{m}}$ vs. L_{AGN} relation now for the whole galaxy sample and calculated in five different redshifts bins (solid lines). For the calculation of the average $\nu L_{60\mu\text{m}}$ we use the complete sample of galaxies at a given redshift without imposing any FIR luminosity cut. Our predictions are compared with the observational results from the PACS Evolutionary Probe (PEP) Herschel survey for the mean FIR emission of X-ray selected AGN at $0.4 \leq z \leq 2.1$ (Rosario et al. 2012). Also shown is the average FIR emission of local ($z = 0$) X-ray selected AGN from the Swift-BAT sample (Cusumano et al. 2010). The straight dashed line has a slope of 0.8 ($\nu L_{60\mu\text{m}} \propto L_{\text{AGN}}^{0.8}$) and shows the correlation line connecting various observational datasets on the SFR – L_{AGN} plane in Netzer 2009. These datasets include type-II SDSS AGN ($0.1 \leq z \leq 0.7$ and $L_{\text{bol}} \gtrsim 10^{42} \text{ erg s}^{-1}$) and Spitzer type-I quasars at $z \sim 1$ (Netzer et al. 2007) and $z = 2 - 3$ (Lutz et al. 2008). Interestingly, the predic-

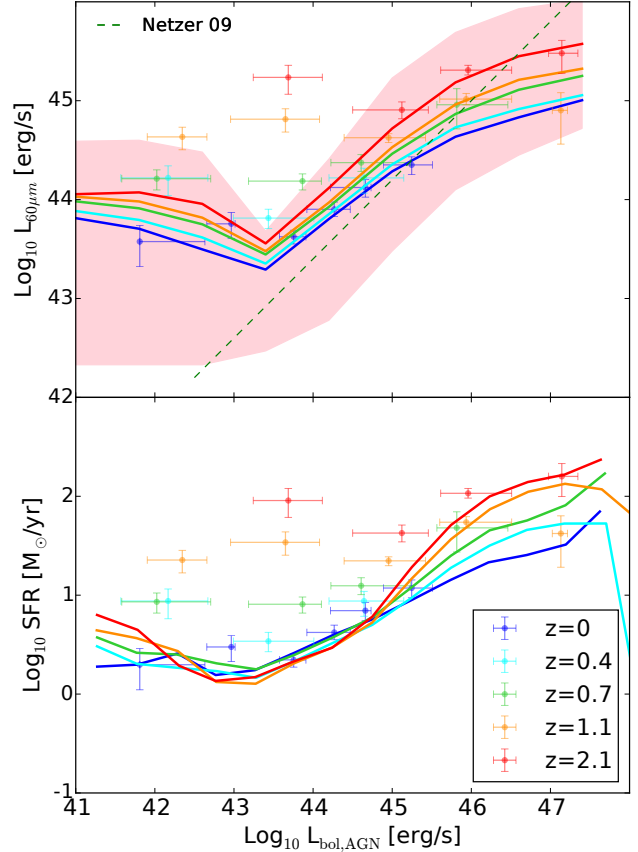


Figure 3. *Top:* Average FIR emission at 60 μm as a function of AGN bolometric luminosity, L_{bol} , for all galaxies in our model. Different lines indicate different redshifts as indicated by the key. The shaded area represents the 10-90 percentiles for the model at $z=2.1$ (pink), but percentiles are similar at all redshifts. Points with error bars show the observed $\nu L_{60\mu\text{m}} - L_{\text{bol}}$ correlation in Rosario et al. (2012), where the $z = 0$ data are from Swift-BAT. The solid-dashed line represents the correlation line connecting various AGN datasets (SDSS type-II AGN with $0.1 \leq z \leq 0.7$ and $L_{\text{bol}} \gtrsim 10^{42} \text{ erg s}^{-1}$, and Spitzer/IRS type-I quasars at $z \sim 0.1$ and $z = 2 - 3$) on the SFR – L_{bol} plane in Netzer (2009). *Bottom:* The predicted SFR- L_{bol} correlation as solid lines at different redshifts. We convert the Rosario et al. data points into SFRs according to Neistein & Netzer (2014).

tions of GALFORM for the $\nu L_{60\mu\text{m}} - L_{\text{AGN}}$ correlation show the same behaviour at all redshifts: for AGN with bolometric luminosities below $10^{43} \text{ erg s}^{-1}$ there is a negative correlation between SF and L_{AGN} , while the trend is reversed (e.g. positive correlation) for higher luminosities.

Our model agrees well with the Swift-BAT data at $z = 0$. In addition, the predicted trend for high luminosity AGN, i.e. $L_{\text{AGN}} \gtrsim 10^{43} \text{ erg s}^{-1}$, follows the slope of the correlation line by Netzer, although the model flattens mildly in the regime of the brightest quasars. Moreover, the GALFORM results at $L_{\text{AGN}} \gtrsim 10^{44} \text{ erg s}^{-1}$ follow the observational data from Rosario et al. . Both Rosario et al. 2012 and Stanley et al. 2015 note an increase in $\nu L_{60\mu\text{m}}$ at higher L_{AGN} , albeit the increase is weaker in Stanley et al. 2015. Our model does predict a moderate increase of SFR towards higher L_{AGN} . In our case, this is due to the fact that the high AGN lu-

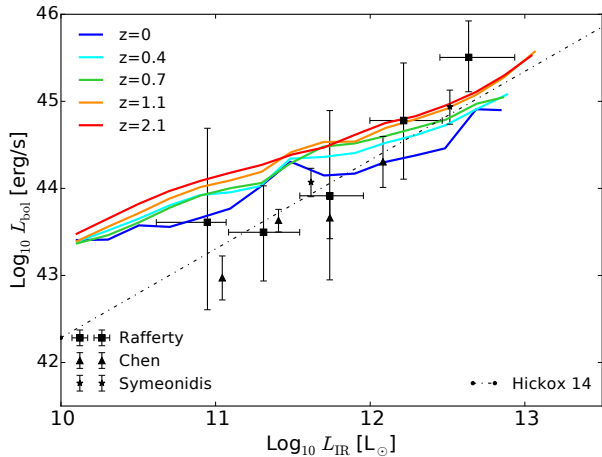


Figure 4. Average AGN bolometric luminosity, L_{bol} , as a function of L_{IR} ($8 - 1000\mu\text{m}$), to allow a direct comparison with the observational data. Different redshifts are shown by different colours, as indicated by the key. Points with error bars show the observational data by Rafferty et al. (2011), Chen et al. (2013), and Symeonidis et al. (2011). The dot-dashed line represents the predictions of the theoretical model presented in Hickox et al. (2014).

minosity end is dominated by the starburst mode where a strong correlation between SFR and L_{AGN} is assumed (see section 2.1).

However, at lower luminosities and higher redshifts the model diverges from observations. There is a pronounced dip in the model at around $L_{\text{AGN}} \approx 10^{43} \text{ erg s}^{-1}$, apparently where the model’s two modes coincide (see figure 2), potentially an artifact of the abrupt transition between the two modes. The negative trend at low luminosities is not visible at all in the data from Rosario et al. (2012), which are practically flat at all redshifts. This observed flat correlation was used in previous studies (Rosario et al.; Mullaney et al.) as a hint of a possible disjoint evolution of BHs and their host galaxies, contrary to what is commonly assumed in many models of galaxy formation. Here we find that in **GALFORM**, this lower luminosity regime is purely shaped by the strong correlation between AGN activity and galaxy evolution.

We also show in the same plot (lower panel) the correlation between AGN luminosity and average SFR for the same sample of galaxies shown in the top panel. The Herschel observational data have now been divided by $1.9 \times 10^{43} \text{ erg s}^{-1}$ to convert the observed the $60\mu\text{m}$ flux into a rough estimation for the SFR (Neistein & Netzer 2014). The model predictions show a behaviour similar to the $\nu L_{60\mu\text{m}} - L_{\text{AGN}}$ correlation shown in the top panel, though the disagreement with the observational data is now more evident. We note however, that our estimate of the observed SFR is only a crude approximation, and therefore this comparison with the model predictions is only for illustrative purposes.

Finally, we plot in Fig. 4 the average AGN luminosity L_{AGN} as a function of the total FIR luminosity L_{IR} . Our predictions are compared to recent observational data (Rafferty et al. 2011; Symeonidis et al. 2011 and Chen et al. 2013) and the AGN variability model proposed by Hickox et al. 2014. Our model predictions are in moderate agreement with the observational results, as well as with the

model proposed by Hickox et al. (even though the SFR and AGN activity are fully and directly coupled in **GALFORM** without any AGN variability). The $L_{\text{IR}} - L_{\text{AGN}}$ correlation predicted by the model is entirely shaped by the starburst mode, (this is in agreement with the observed correlation between SMBH growth rate and the SFR reported by Mullaney et al. 2012a). In contrast to the predictions shown in Fig. 3, we now find a monotonically increasing correlation. The average L_{AGN} luminosity is dominated by those galaxies undergoing starburst-mode AGN activity, and thus the slope of the correlation reflects the slope of the starburst-mode branch in Fig. 2. This is because the typical AGN luminosities of these galaxies, and also their number density, are much higher than the ones of galaxies in the hot-halo mode branch.

3.3 Properties of AGN hosts

The $L_{\text{AGN}} - L_{\text{IR}}$ correlation can in principle provide insights into the host properties of AGN and thus, impose constraints on theoretical models of galaxy formation. For example Rosario et al. suggest that the flatness of the correlation, $L_{\text{AGN}} - \nu L_{60\mu\text{m}}$, at low AGN luminosities and its steep evolution at higher luminosities indicates two regimes of AGN activity. What our results show is that these two AGN regimes happen in very different galaxy populations.

AGN at the bright end of the $L_{\text{AGN}} - \nu L_{60\mu\text{m}}$ correlation shown in Fig. 3 are found in bursty systems experiencing intense SF. The hosts of these luminous AGN are gas rich systems living in $\sim 10^{12} M_{\odot}$ DM halos, and are similar to actively star forming galaxies. In contrast, in the faint L_{AGN} region of the plane we find galaxies whose central BHs accrete predominately via the hot-halo mode. As already mentioned, this mode is particularly prominent in more massive systems ($\gtrsim 10^{13} M_{\odot}$), where AGN feedback efficiently suppresses gas cooling and SF. The typical host of an AGN in that region would be a spheroidal system that at low redshifts resembles an early-type galaxy.

The stellar masses of the galaxies populating the $L_{\text{AGN}} - L_{\text{IR}}$ plane span a wide range of values (see Fanidakis et al. 2013b). We show this in Fig. 5, where we plot the SFR as a function of stellar mass at $z = 0$ for active and inactive galaxies in our model. We define as inactive all galaxies with $L_{\text{AGN}} < 10^{41} \text{ erg/s}$. At the same time, we split active galaxies into faint ($10^{41} < L_{\text{AGN}} < 10^{43} \text{ erg/s}$) and bright AGN ($L_{\text{AGN}} > 10^{43} \text{ erg/s}$). The transition luminosity from faint to bright AGN approximately marks the break in the $L_{\text{AGN}} - \nu L_{60\mu\text{m}}$ correlation shown in Fig. 3. We refer the reader to Lagos et al. (2011) for the overall properties of galaxies on the $M_{\text{star}} - SFR$ plane in **GALFORM**.

What is immediately evident from Fig. 5 is that AGN and inactive galaxies populate the same regions on the $M_{\text{star}} - SFR$ plane. Bright AGN are predominately found on the main sequence, though the scatter is strong. AGN in this sample are powered by accretion during the starburst mode. On the other hand, faint AGN are found both on the main sequence, but also immediately below it, i.e. in the region of passive galaxies. AGN hosts in the passive regime are typically quenched and have low SFRs. In the faint AGN sample we find AGN powered by both the starburst (AGN in the main sequence) and the hot-halo mode (AGN in the passive regime). Overall, we find no particular feature, e.g.

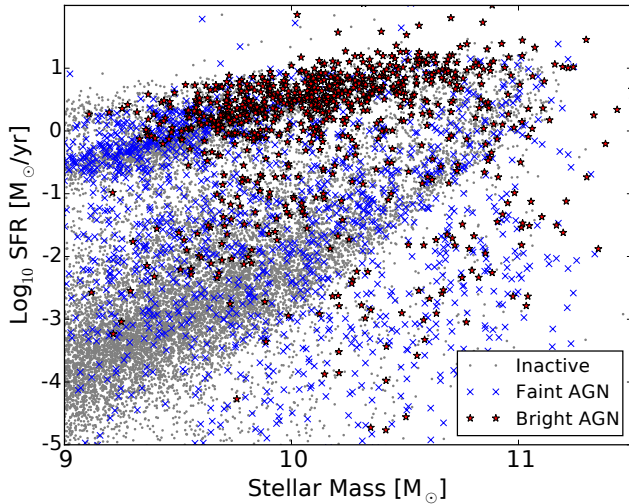


Figure 5. Stellar mass - star formation rate plane at $z = 0$ for an unbiased subset of model galaxies in three bins: *inactive*: $L_{\text{AGN}} < 10^{41}$ erg/s, *faint AGN*: $10^{41} < L_{\text{AGN}} < 10^{43}$ erg/s, *bright AGN*: $L_{\text{AGN}} > 10^{43}$ erg/s

green valley, in the distribution of AGN. A detailed comparison between active and inactive galaxies could potentially reveal differences in the two galaxy populations, but this exercise is beyond the scope of this study. We finally note that the $M_{\text{star}} - \text{SFR}$ plane at higher redshifts, ($z \sim 2$) is characterised by the absence of the passive regime (for both active and inactive galaxies). The bimodal distribution of AGN at $z = 0$ is linked to the quenching of galaxies in the low-redshift universe and relates strongly to the colour bimodality of AGN in GALFORM, as shown in Georgakakis et al. (2014).

To gain more insight into the SF properties of AGN hosts, we show in the top panels of Fig. 6, the molecular hydrogen gas content as a function of AGN luminosity for a small subset of galaxies at $z = 0$ and $z = 2.1$. We remind the reader that the molecular hydrogen content is calculated following Lagos et al. (2011), where the molecular-to-total gas ratio increases with the mid-plane hydrostatic pressure of the galactic disk. What is immediately evident in this plot is that both at high and low redshifts the hosts of faint and bright AGN reach similarly high molecular gas contents, but with a larger scatter towards lower values in faint AGN hosts at $z = 0$. At a first look, this is surprising given that the hosts of faint AGN tend to be more passive systems. Indeed, the total cold gas reservoirs of early-type galaxies are lower than those of starbursts in our model. Yet, the model predicts a strong correlation between the molecular-to-atomic hydrogen ratio with increasing bulge-to-total ratio, meaning that early type galaxies are relatively richer in molecular hydrogen compared to atomic hydrogen, as implied also by past and recent observations (Young & Knezek 1989; Bettoni et al. 2003; Leroy et al. 2008; Lisenfeld et al. 2011; Boselli et al. 2014). This is due to the higher compactness of early-type galaxies compared to starburst galaxies, which results in higher gas pressure and thus, higher molecular-to-atomic hydrogen ratios (Lagos et al. 2014b).

Despite the high H_2 mass in early-type galaxies, the SFR in these systems remains low compared to starburst

galaxies, as has already been shown in the lower panel of Fig. 3. At high redshift this is due to the different timescales for star formation between spheroidals and starburst systems, with the latter ones having shorter timescales (see also section 2.3). At low redshifts, early-type galaxies, i.e. bulge-dominated systems, tend to have relatively low mean SFRs due to their lower mean molecular gas contents. This is also shown in the lower panel of Fig. 6, where we now plot the specific SFR (sSFR).

Similarly to the SFR, the AGN luminosity is also low in early-type galaxies. This is due to the fact that these systems are dynamically stable, having very subdominant disks. They rarely undergo disk instabilities and thus, quasar-like AGN activity is never achieved (though major mergers could occasionally produce significant accretion). BHs typically grow via the hot-halo mode, which in the redshift regime of interest always produces low density accretion flows, irrespective of the gas reservoir of the galaxy. In contrast, in the high-luminosity regime we find gas-rich starburst galaxies that often experience disk instabilities which then trigger efficient and quasar-like accretion onto their central BHs.

Our results suggest that galaxies in the low luminosity region of the $L_{\text{AGN}} - \nu L_{60\mu\text{m}}$ plane are less efficient *both* at building stars and growing BHs than their high luminosity counterparts.

4 DISCUSSION

Overall our model produces a SFR- L_{AGN} relation that is in reasonable agreement with observations, especially taking into account that no parameters of the model were tuned to reproduce this specific observational relation. As it can be seen in Fig. 2, the model predicts FIR luminosities for the faint and moderate luminosity AGN that match those observed in the Herschel surveys. In addition, the model provides a reasonably good fit to the FIR luminosity function of the total galaxy (Lacey et al. in prep) and AGN population (Fanidakis et al. 2012). Note that Rosario et al. use stacking to estimate the FIR flux for sources whose flux is below the 3σ detection limit of the PACS instrument. Therefore, there is in principle no reason to create a mock catalogue for mimicking flux limits and biases related to the observations. Thus, assuming that their data sample is complete, possible reasons for the disagreement could be the following. First of all, there could be a strong contribution in the model of very faint FIR sources to the average $\nu L_{60\mu\text{m}}$ value.

As we have already mentioned, the objects populating this region of the plot are identified with early type galaxies. These systems are passive in terms of their efficiency in forming of stars (although occasionally a starburst could occur as a consequence of a major merger), and therefore their SFR and, as a consequence, their FIR emission depend on the H_2 gas reservoir (Lagos et al. 2011). However, the model seems to produce a few too many low mass systems that are also low in cold gas (atomic and molecular) and thus have low SFR. But based on previous work with this model (Lagos et al. 2012, 2014a,b, also Lacey et al. in prep.), the FIR luminosities and SFRs in the vertical axes of Fig. 3 should be in principle consistent with the observations.

A more plausible reason for the strong disagreement could be the simplicity of the assumptions for the triggering

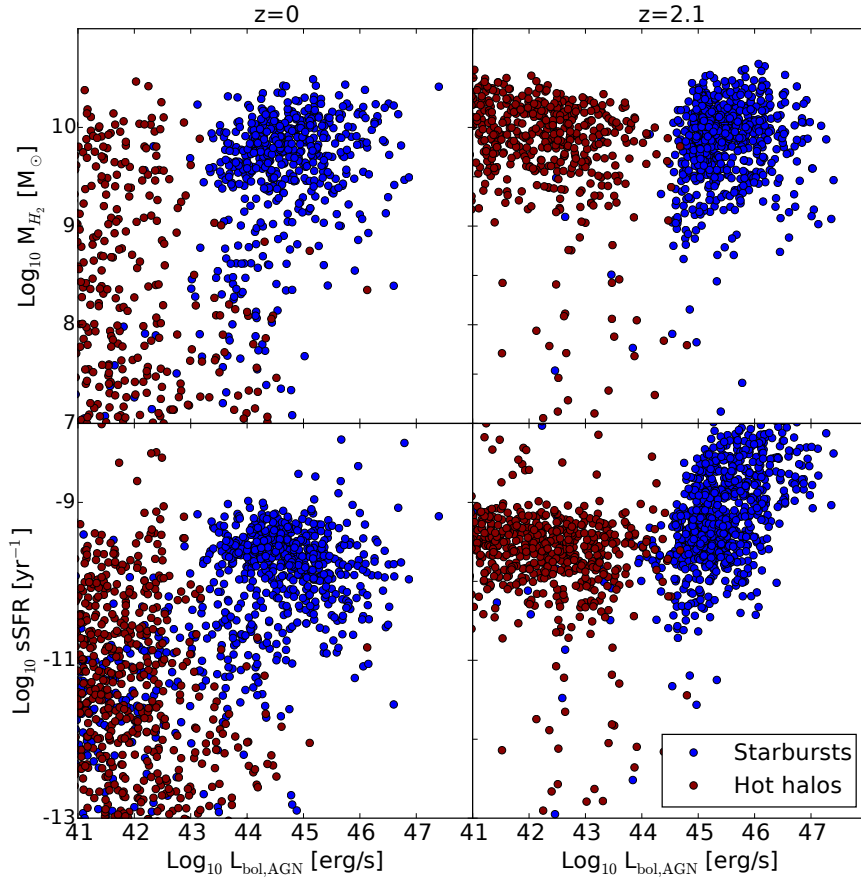


Figure 6. *Top:* Predicted molecular hydrogen mass, M_{H_2} , as a function of bolometric AGN luminosity for 4,000 randomly selected galaxies at $z = 0$ (left) and $z = 2.1$ (right). Galaxies in which the central BH experiences starburst-mode activity are shown in blue, while those with BHs growing during the hot-halo mode in red. *Bottom:* Predicted specific SFR (SFR/ M_*) as a function of AGN luminosity. Colors and redshifts as at the top panel. We only show galaxies with stellar masses above $10^{10} M_{\odot}$.

and variability of AGN activity. In **GALFORM**, AGN activity begins with the onset of star formation in a starburst without a time delay. A possible delay between the triggering of AGN activity and the formation of stars in a burst could result into a decrease towards lower AGN luminosities for the objects populating the bright AGN regime of the diagram. The incorporation of an AGN variability model could have a similar effect. AGN luminosities are calculated assuming a constant accretion rate. Thus, the luminosity is constant during the entire course of accretion. However, AGN are known to exhibit strong variability on a wide range of timescales (Novak et al. 2011).

Recently, Hickox et al. presented a model in which SF and BH accretion are closely connected over long timescales, but that short-term AGN variability can wash out this correlation for low to moderate L_{AGN} . Here, despite the fact that the **GALFORM** intrinsic FIR-AGN relation is driven by completely different phenomena, the inclusion of AGN variability could improve the agreement with the observations simply by shifting some bright quasars to lower AGN luminosities.

A final explanation for the disagreement with the observations at lower AGN luminosity could be that the AGN luminosities we calculate for the AGN in the hot-halo mode are underpredicted (see also discussion about the hot-halo

AGN in Krumpe et al. in prep). Indeed, the sharp transition from the hot-halo mode to the starburst mode, which appears as a strong break at $L_{AGN} \sim 10^{43} \text{ erg s}^{-1}$ in the $L_{AGN} - \nu L_{60\mu\text{m}}$ correlation, could possibly be smoothed out if the hot-halo AGN luminosities were systematically higher. In the current version of the model, the hot-halo luminosity is calculated directly from the cooling properties of the host DM halo, via the expression $\dot{M} = L_{\text{cool}} / (\epsilon_{\text{kin}} c^2)$. While L_{cool} is well defined in the model, the value of the efficiency parameter ϵ_{kin} is loosely constrained, mainly by requiring the model to reproduce the BH mass function in the local Universe. By boosting the luminosity of hot-halo AGN we could in principle make the transition from one regime to the other smoother and thus obtain a better agreement with the data. We note however that our aim in this paper is merely to report what observable correlations are predicted by a model in which BH and SFR are strongly coupled. We made no adjustments to the model in preparation for doing this analysis. Nevertheless, it is interesting that a comparison with FIR observations of X-ray selected AGN could provide possible constraints in the modelling of AGN feedback in galaxy formation models.

5 CONCLUSIONS

In the current paradigm of galaxy formation the triggering mechanisms of AGN activity are often responsible for initiating intense SF in the host galaxy. At the same time, it is widely accepted, yet unproven, that AGN activity is the main driver of the quenching of SF in massive galaxies (Di Matteo et al. 2005, Monaco & Fontanot 2005). In both cases, a correlation between observable proxies for SF and AGN activity is somehow expected. However, several recent observational studies have shown that there is little (Rosario et al. 2012) or practically no correlation (Mullaney et al. 2012b; Stanley et al. 2015) between FIR luminosity and the AGN luminosity. These results have been seen as a challenge for current galaxy formation models.

In this study, we have reported the predictions of the semi-analytic model **GALFORM** for the connection between SFR and AGN activity. **GALFORM** calculates AGN properties by tracking the BH accretion rate and the evolution of BH mass and spin. BHs grow via cold gas accretion (starburst mode), usually triggered by disk instabilities or galaxy mergers, and by hot-gas accretion (hot-halo mode), typically in massive quasi-hydrostatic haloes that are subject to AGN feedback. During the course of accretion the **GALFORM** code calculates various AGN properties, as for example the disk emission in different bands, by considering the dependence of the bolometric disk emission on the structure of the accretion disk.

Galaxies in **GALFORM** build stars in disks from molecular hydrogen. When a galaxy experiences a disk instability or galaxy merger all the available cold gas (atomic and molecular) turns into stars via a burst. The growth of BHs is strongly linked to the buildup of stars. During a burst of SF a fraction of the gas that turns into stars is accreted onto the BH (starburst mode). This creates a strong correlation between SFR and AGN luminosity. In galaxies found in more massive, quasi-hydrostatic haloes SF is less efficient. The accretion power couples with the cooling properties of the gas in the halo resulting in a suppression of gas cooling and a regulation of the SF. This gives rise to an anti-correlation between SFR and AGN activity.

To compare our predictions to recent Herschel observations for the mean SFR of X-ray selected AGN we compute the properties of galaxies in the FIR. The FIR emission in our model is due to the reprocessing by dust of the incident stellar continuum radiation. The resulting emission at $60\ \mu\text{m}$, $\nu L_{60\mu\text{m}}$, scales nearly linearly with SFR (Fig. 1), and thus represents a good tracer for the SFR. For the brightest AGN, **GALFORM** predicts a strong correlation between L_{bol} and $\nu L_{60\mu\text{m}}$, which arises from the strong coupling of the BH accretion to starbursts. For faint and intermediate luminosity AGN, the model predicts a mildly negative correlation, which is a consequence of the negative feedback effect these AGN have on their host galaxies. When compared to the Herschel PACS data for X-ray selected AGN in the COSMOS and GOODS-S/N fields we find a very good agreement in the bright AGN luminosity regime. In the low-luminosity regime we find that the model systematically underpredicts the average $\nu L_{60\mu\text{m}}$.

Finally, we showed that the objects populating the bright and faint regimes of the $L_{\text{bol}} - \nu L_{60\mu\text{m}}$ plane represent different classes of galaxies. In the high luminosity regime

we find gas-rich disk galaxies, that recently underwent a disk instability, and now exhibit strong starbursts and prodigious BH growth and AGN activity. In the low luminosity regime, we find massive early-type galaxies that experience quiescent SF, BH growth and AGN activity. Interestingly, despite the fact that these galaxies are subject to AGN feedback, many reach relatively large masses of molecular hydrogen. In fact, we find that their H_2 reservoirs at high redshift are similar to the gas-rich disk galaxies in the high luminosity regime of the diagram. These galaxies, however, are inefficient in building stars as can be seen in their sSFRs. We find that their SFRs and FIR luminosities tend to be on average approximately one order of magnitude lower than the galaxies in the bright luminosity regime. Nevertheless, a large fraction reach high molecular hydrogen masses, so a large population of low AGN luminosity galaxies should have as bright CO emission as their high-AGN luminosity counterparts.

Future observations of the molecular gas/CO emission in X-ray selected AGN will help to further disentangle the SFR-AGN correlation. Until then, we hope that this work will provide adequate motivation that AGN activity remains a viable solution to explain the origin of red-and-dead galaxies.

ACKNOWLEDGMENTS

The authors would like to thank David Rosario for providing the observational data in Fig. 3. Also many thanks to Roberto Decarli for important guidance and discussions. TAG and AVM acknowledge funding by Sonderforschungsbereich SFB 881 The Milky Way System (subproject A1) of the German Research Foundation (DFG).

REFERENCES

- Baugh C. M., Lacey C. G., Frenk C. S., Granato G. L., Silva L., Bressan A., Benson A. J., Cole S., 2005, MNRAS, 356, 1191
- Bettoni D., Galletta G., García-Burillo S., 2003, A&A, 405, 5
- Blitz L., Rosolowsky E., 2006, ApJ, 650, 933
- Booth C. M., Schaye J., 2009, MNRAS, 398, 53
- Boselli A., Cortese L., Boquien M., Boissier S., Catinella B., Lagos C., Saintonge A., 2014, A&A, 564, A66
- Bower R. G., Benson A. J., Malbon R., Helly J. C., Frenk C. S., Baugh C. M., Cole S., Lacey C. G., 2006, MNRAS, 370, 645
- Bressan A., Granato G. L., Silva L., 1998, A&A, 332, 135
- Cattaneo A., 2001, MNRAS, 324, 128
- Chen C.-T. J., Hickox R. C., Alberts S., Brodwin M., Jones C., Murray S. S., Alexander D. M., Assef R. J., Brown M. J. I., Dey A., Forman W. R., Gorjian V., Goulding A. D., Le Floc'h E., Jannuzi B. T., Mullaney J. R., Pope A., 2013, ApJ, 773, 3
- Cole S., Lacey C. G., Baugh C. M., Frenk C. S., 2000, MNRAS, 319, 168
- Croton D. J., Springel V., White S. D. M., De Lucia G., Frenk C. S., Gao L., Jenkins A., Kauffmann G., Navarro J. F., Yoshida N., 2006, MNRAS, 365, 11

- Cusumano G., La Parola V., Segreto A., Ferrigno C., Maselli A., Sbarufatti B., Romano P., Chincarini G., Giommi P., Masetti N., Moretti A., Parisi P., Tagliaferri G., 2010, *A&A*, 524, A64
- Di Matteo T., Colberg J., Springel V., Hernquist L., Sijacki D., 2008, *ApJ*, 676, 33
- Di Matteo T., Springel V., Hernquist L., 2005, *Nature*, 433, 604
- Elmegreen B. G., 1993, *ApJ*, 419, L29
- Fanidakis N., Baugh C. M., Benson A. J., Bower R. G., Cole S., Done C., Frenk C. S., 2011, *MNRAS*, 410, 53
- Fanidakis N., Baugh C. M., Benson A. J., Bower R. G., Cole S., Done C., Frenk C. S., Hickox R. C., Lacey C., Del P. Lagos C., 2012, *MNRAS*, 419, 2797
- Fanidakis N., Georgakakis A., Mountrichas G., Krumpel M., Baugh C. M., Lacey C. G., Frenk C. S., Miyaji T., Benson A. J., 2013a, *MNRAS*, 435, 679
- Fanidakis N., Macciò A. V., Baugh C. M., Lacey C. G., Frenk C. S., 2013b, *MNRAS*, 436, 315
- Ferrara A., Bianchi S., Cimatti A., Giovanardi C., 1999, *ApJS*, 123, 437
- Ferrarese L., Merritt D., 2000, *ApJ*, 539, L9
- Gebhardt K., Bender R., Bower G., Dressler A., Faber S. M., Filippenko A. V., Green R., Grillmair C., Ho L. C., Kormendy J., Lauer T. R., Magorrian J., Pinkney J., Richstone D., Tremaine S., 2000, *ApJ*, 539, L13
- Georgakakis A., Pérez-González P. G., Fanidakis N., Salvato M., Aird J., Messias H., Lotz J. M., Barro G., Hsu L.-T., Nandra K., Rosario D., Cooper M. C., Kocevski D. D., Newman J. A., 2014, *MNRAS*, 440, 339
- Gonzalez-Perez V., Lacey C. G., Baugh C. M., Frenk C. S., Wilkins S. M., 2013, *MNRAS*, 429, 1609
- Gonzalez-Perez V., Lacey C. G., Baugh C. M., Lagos C. D. P., Helly J., Campbell D. J. R., Mitchell P. D., 2014, *MNRAS*, 439, 264
- Granato G. L., De Zotti G., Silva L., Bressan A., Danese L., 2004, *ApJ*, 600, 580
- Guo Q., White S., Boylan-Kolchin M., De Lucia G., Kauffmann G., Lemson G., Li C., Springel V., Weinmann S., 2011, *MNRAS*, 413, 101
- Harrison C. M., Alexander D. M., Swinbank A. M., Smail I., Alaghband-Zadeh S., Bauer F. E., Chapman S. C., Del Moro A., Hickox R. C., Ivison R. J., Menéndez-Delmestre K., Mullaney J. R., Nesvadba N. P. H., 2012, *MNRAS*, 426, 1073
- Hickox R. C., Mullaney J. R., Alexander D. M., Chen C.-T. J., Civano F. M., Goulding A. D., Hainline K. N., 2014, *ApJ*, 782, 9
- Hopkins P. F., Richards G. T., Hernquist L., 2007, *ApJ*, 654, 731
- Jahnke K., Macciò A. V., 2011, *ApJ*, 734, 92
- Kauffmann G., Haehnelt M., 2000, *MNRAS*, 311, 576
- Kim H.-S., Baugh C. M., Benson A. J., Cole S., Frenk C. S., Lacey C. G., Power C., Schneider M., 2011, *MNRAS*, 414, 2367
- Komatsu E., Smith K. M., Dunkley J., Bennett C. L., Gold B., Hinshaw G., Jarosik N., Larson D., Nolte M. R., Page L., Spergel D. N., Halpern M., Hill R. S., Kogut A., Limon M., Meyer S. S., Odegard N., Tucker G. S., Weiland J. L., Wollack E., Wright E. L., 2011, *ApJS*, 192, 18
- Lacey C. G., Baugh C. M., Frenk C. S., Benson A. J., 2011, *MNRAS*, 412, 1828
- Lacey C. G., Baugh C. M., Frenk C. S., Benson A. J., Orsi A., Silva L., Granato G. L., Bressan A., 2010, *MNRAS*, 405, 2
- Lagos C. D. P., Baugh C. M., Zwaan M. A., Lacey C. G., Gonzalez-Perez V., Power C., Swinbank A. M., van Kampen E., 2014a, *MNRAS*, 440, 920
- Lagos C. d. P., Bayet E., Baugh C. M., Lacey C. G., Bell T. A., Fanidakis N., Geach J. E., 2012, *MNRAS*, 426, 2142
- Lagos C. d. P., Davis T. A., Lacey C. G., Zwaan M. A., Baugh C. M., Gonzalez-Perez V., Padilla N. D., 2014b, *MNRAS*, 443, 1002
- Lagos C. D. P., Lacey C. G., Baugh C. M., Bower R. G., Benson A. J., 2011, *MNRAS*, 416, 1566
- Leroy A. K., Walter F., Brinks E., Bigiel F., de Blok W. J. G., Madore B., Thornley M. D., 2008, *AJ*, 136, 2782
- Lisenfeld U., Espada D., Verdes-Montenegro L., Kuno N., Leon S., Sabater J., Sato N., Sulentic J., Verley S., Yun M. S., 2011, *A&A*, 534, A102
- Lutz D., Mainieri V., Rafferty D., Shao L., Hasinger G., Weiß A., Walter F., Smail I., Alexander D. M., Brandt W. N., Chapman S., Coppin K., Förster Schreiber N. M., Gawiser E., Genzel R., Greve T. R., Ivison R. J., Koekemoer A. M., Kurczynski P., Menten K. M., Nordon R., Popesso P., Schinnerer E., Silverman J. D., Wardlow J., Xue Y. Q., 2010, *ApJ*, 712, 1287
- Lutz D., Sturm E., Tacconi L. J., Valiante E., Schweitzer M., Netzer H., Maiolino R., Andreani P., Shemmer O., Veilleux S., 2008, *ApJ*, 684, 853
- Mahadevan R., 1997, *ApJ*, 477, 585
- Monaco P., Fontanot F., 2005, *MNRAS*, 359, 283
- Mullaney J. R., Daddi E., Béthermin M., Elbaz D., Juneau S., Pannella M., Sargent M. T., Alexander D. M., Hickox R. C., 2012a, *ApJ*, 753, L30
- Mullaney J. R., Pannella M., Daddi E., Alexander D. M., Elbaz D., Hickox R. C., Bournaud F., Altieri B., Aussel H., Coia D., Dannerbauer H., Dasyra K., Dickinson M., Hwang H. S., Kartaltepe J., Leiton R., Magdis G., Maggelli B., Popesso P., Valtchanov I., Bauer F. E., Brandt W. N., Del Moro A., Hanish D. J., Ivison R. J., Juneau S., Luo B., Lutz D., Sargent M. T., Scott D., Xue Y. Q., 2012b, *MNRAS*, 419, 95
- Narayan R., Yi I., 1994, *ApJ*, 428, L13
- Neistein E., Netzer H., 2014, *MNRAS*, 437, 3373
- Netzer H., 2009, *MNRAS*, 399, 1907
- Netzer H., Lutz D., Schweitzer M., Contursi A., Sturm E., Tacconi L. J., Veilleux S., Kim D.-C., Rupke D., Baker A. J., Dasyra K., Mazzarella J., Lord S., 2007, *ApJ*, 666, 806
- Novak G. S., Ostriker J. P., Ciotti L., 2011, *ApJ*, 737, 26
- Okamoto T., Nemmen R. S., Bower R. G., 2008, *MNRAS*, 385, 161
- Orsi A., Lacey C. G., Baugh C. M., Infante L., 2008, *MNRAS*, 391, 1589
- Rafferty D. A., Brandt W. N., Alexander D. M., Xue Y. Q., Bauer F. E., Lehmer B. D., Luo B., Papovich C., 2011, *ApJ*, 742, 3
- Robertson B., Bullock J. S., Cox T. J., Di Matteo T., Hernquist L., Springel V., Yoshida N., 2006, *ApJ*, 645, 986
- Rodighiero G., Brusa M., Daddi E., Negrello M., Mullaney J. R., Delvecchio I., Lutz D., Renzini A., Franceschini A., Baronchelli I., Pozzi F., Gruppioni C., Strazzullo V.,

- Cimatti A., Silverman J., 2015, *ApJ*, 800, L10
- Rosario D. J., Santini P., Lutz D., Shao L., Maiolino R., Alexander D. M., Altieri B., Andreani P., Aussel H., Bauer F. E., Berta S., Bongiovanni A., Brandt W. N., Brusa M., Cepa J., Cimatti A., Cox T. J., Daddi E., Elbaz D., Fontana A., Förster Schreiber N. M., Genzel R., Grazian A., Le Floch E., Magnelli B., Mainieri V., Netzer H., Nordon R., Pérez García I., Poglitsch A., Popesso P., Pozzi F., Riguccini L., Rodighiero G., Salvato M., Sanchez-Portal M., Sturm E., Tacconi L. J., Valtchanov I., Wuyts S., 2012, *A&A*, 545, A45
- Schaye J., Crain R. A., Bower R. G., Furlong M., Schaller M., Theuns T., Dalla Vecchia C., Frenk C. S., McCarthy I. G., Helly J. C., Jenkins A., Rosas-Guevara Y. M., White S. D. M., Baes M., Booth C. M., Camps P., Navarro J. F., Qu Y., Rahmati A., Sawala T., Thomas P. A., Trayford J., 2015, *MNRAS*, 446, 521
- Shakura N. I., Sunyaev R. A., 1973, *A&A*, 24, 337
- Shao L., Lutz D., Nordon R., Maiolino R., Alexander D. M., Altieri B., Andreani P., Aussel H., Bauer F. E., Berta S., Bongiovanni A., Brandt W. N., Brusa M., Cava A., Cepa J., Cimatti A., Daddi E., Dominguez-Sanchez H., Elbaz D., Förster Schreiber N. M., Geis N., Genzel R., Grazian A., Gruppioni C., Magdis G., Magnelli B., Mainieri V., Pérez García A. M., Poglitsch A., Popesso P., Pozzi F., Riguccini L., Rodighiero G., Rovilos E., Saintonge A., Salvato M., Sanchez Portal M., Santini P., Sturm E., Tacconi L. J., Valtchanov I., Wetzstein M., Wiegrecht E., 2010, *A&A*, 518, L26
- Sijacki D., Springel V., Di Matteo T., Hernquist L., 2007, *MNRAS*, 380, 877
- Silk J., Rees M. J., 1998, *A&A*, 331, L1
- Silva L., Granato G. L., Bressan A., Danese L., 1998, *ApJ*, 509, 103
- Somerville R. S., Hopkins P. F., Cox T. J., Robertson B. E., Hernquist L., 2008, *MNRAS*, 391, 481
- Springel V., Di Matteo T., Hernquist L., 2005a, *MNRAS*, 361, 776
- Springel V., White S. D. M., Jenkins A., Frenk C. S., Yoshida N., Gao L., Navarro J., Thacker R., Croton D., Helly J., Peacock J. A., Cole S., Thomas P., Couchman H., Evrard A., Colberg J., Pearce F., 2005b, *Nature*, 435, 629
- Stanley F., Harrison C. M., Alexander D. M., Swinbank A. M., Aird J. A., Del Moro A., Hickox R. C., Mullaney J. R., 2015, *ArXiv e-prints*
- Symeonidis M., Georgakis A., Seymour N., Auld R., Bock J., Brisbin D., Buat V., Burgarella D., Chaniel P., Clements D. L., Cooray A., Eales S., Farrah D., Franceschini A., Glenn J., Griffin M., Hatziminaoglou E., Ibar E., Ivison R. J., Mortier A. M. J., Oliver S. J., Page M. J., Papageorgiou A., Pearson C. P., Pérez-Fournon I., Pohlen M., Rawlings J. I., Raymond G., Rodighiero G., Roseboom I. G., Rowan-Robinson M., Scott D., Smith A. J., Tugwell K. E., Vaccari M., Vieira J. D., Vigroux L., Wang L., Wright G., 2011, *MNRAS*, 417, 2239
- Vogelsberger M., Genel S., Springel V., Torrey P., Sijacki D., Xu D., Snyder G., Nelson D., Hernquist L., 2014, *MNRAS*, 444, 1518
- Young J. S., Knezek P. M., 1989, *ApJ*, 347, L55

This paper has been typeset from a \TeX / \LaTeX file prepared by the author.